Dynamic response of a double-deck circular tunnel embedded in a full-space

Arnau Clot[a,*], Robert Arcos[a], Jordi Romeu[a], Teresa Pàmies[a]

[a] *Acoustical and Mechanical Engineering Laboratory (LEAM). Universitat Politècnica de Catalunya, Spain*

Abstract

A three-dimensional dynamic model for calculating the ground-borne vibrations generated by harmonic loads applied on the interior floor of a double-deck circular tunnel is developed. The response of the system is obtained coupling the interior floor subsystem and the tunnel-soil subsystem in the wavenumber-frequency domain. The interior floor is modeled as a thin plate of infinite length in the train circulation direction and the tunnel-soil system is described using the Pipe in Pipe model. Some numerical instabilities of the resulting expressions are overcome by using analytic approximations. The results show that the dynamic behaviour of the interior floor clearly influences the magnitude of the coupling loads acting on the tunnel structure. The soil response to a harmonic load acting on the double-deck tunnel is compared to the one obtained for the case of a simple tunnel finding significant differences between them for the whole range of frequencies studied. The proposed model extends the prediction of train-induced vibrations using computationally efficient models to this type of tunnel structure.

Keywords: Underground vibrations, Double-deck tunnel, Coupling subsystems, Viscoelastic full-space.

*Corresponding author
Email address: arnau.clot@upc.edu (Arnau Clot)

1. Introduction

In recent years underground train-induced ground-borne vibrations have become a serious issue in heavily populated areas. The increasing importance that this type of infrastructures has in big cities (Broere (2016)) has lead to the need for new predictive models, able to deal with the complexity of the problem. Unfortunately, the implementation of innovative tunnel structure designs brings new difficulties to the efficient prediction of vibration impact. This is the case, for example, of double-deck circular tunnels, a type of tunnel where one or more interior floors divide the structure into different parts and where trains and/or vehicles circulate through them. This type of infrastructure is being or has already been constructed in several cities worldwide, as, for example, Barcelona Metro Line 9, Seattle State Road 99 or Kuala Lumpur SMART tunnel. Some studies have already been carried out for double-deck tunnel structures, such as the determination of its response to nearby tunnelling activities (Li and Yuan (2012)). However, the ground vibrations generated by a double-deck tunnel have not been well studied yet.

Many authors have considered a numerical approach for modelling the track-tunnel-soil system and predicting underground railway induced ground vibrations. Due to the complexity of the problem, two-dimensional (2D) Finite Element Method (FEM) models were initially proposed by Chua et al. (1992). The validity of the plane-strain assumption was studied by Andersen, L. and Jones, C.J.C. (2006), who compared the results obtained with a 2D and with a three-dimensional (3D) FEM-Boundary Element Method (BEM) hybrid model of a non-circular underground tunnel. They concluded that 2D models could not be used to obtain accurate results and that the 3D nature of the problem had to be taken into account. A similar conclusion has been more recently stated by Real et al. (2015), who compared the results obtained with a 3D FEM model calibrated using in situ measurements to those obtained using 2D FEM models, concluding that the former gives more accurate results. The unreasonable computational cost required by a 3D model has been overcome by considering two different simplifying hypotheses. The first one, proposed by Clouteau, D. and Arnst, M. and Al-Hussaini, T. M. and Degrande, G. (2005) and by Degrande et al. (2006), is to assume that the tunnel-soil structure is periodic in the train circulation direction. This periodicity allowed them to develop a 3D periodic FEM-BEM model

that, using the Floquet Transform, requires to mesh only a reference cell in order to find the solution of the problem. The other, initially used by Aubry et al. (1994), is to assume that the geometry and mechanical properties of the tunnel-soil system are invariant in the train circulation direction. With this, the solution can be obtained in the wavenumber domain meshing only a cross-section of the system. Models of this type, usually called two-and-a-half dimensional (2.5D) models, have been proposed, among others, by Sheng et al. (2005), who developed a 2.5D FEM-BEM model of the problem, by Müller et al. (2008), who developed a 2.5D hybrid FEM-analytical model of a non-circular tunnel, and, more recently, by François et al. (2010). An intersting alternative has been used by Nejati, H.R. and Ahmadi, M. and Hashemolhosseini, H. (2012), who presented a 2D Finite Difference Model to compute the surface vibration induced by an underground train. Despite the powerful improvements and simplifications developed, numerical models still require large computational and engineering costs, making them unsuitable in scope or for design stages of a new underground construction. In these cases, the use of analytical or semi-analytical prediction models is usually a better alternative.

The most recognized analytical model for underground ground-borne vibrations is probably the Pipe-in-Pipe (PiP) model, developed by Forrest and Hunt (2006a,b). The initial formulation has been later improved and used for obtaining a wide variety of results. The tunnel-soil model was coupled to a floating-slab track model by Hussein and Hunt (2007). Gupta et al. (2007) compared the model results to those obtained using a coupled FEM-BEM periodic model of the superstructure-tunnel-soil system. Hussein et al. (2006) extended the initial full-space formulation to a half-space one using the full and half-space 2.5D elastodynamic Green's functions obtained by Tadeu and Kausel (2000) and by Tadeu et al. (2001) respectively. The extension to a layered half-space using a fictitious force method has been recently presented by Hussein et al. (2014). The PiP model, however, is currently unable to deal with alternative construction geometries such as the mentioned double-deck tunnel. A 2D power flow comparison performed by Clot et al. (2014) has shown that significant differences are expected to be found between the predicted vibration levels found for this tunnel structure and the ones obtained for a simple tunnel.

The dynamic response of thin plate-thin cylindrical shell structures was ini-

tially studied by Peterson and Boyd (1978), who presented the first analytical model for a shell with a partitioned floor as a simplified model of a plane fuselage. Lee and Choi (2001) later obtained the free vibration response of a simply supported shell-plate structure from the response of their subsystems. The response of both subsystems was calculated using the Rayleigh-Ritz energy method. The model was later extended by Lee et al. (2003) to the case of laminated composites. This approach was also used by Wang et al. (2004) to study the power flow characteristics of the plate-cylindrical shell structure and by Zhao et al. (2012) to study the forced response of a plate-cylindrical shell structure. In all these works the plate-shell structures are finite.

This paper presents a 2.5D semianalytical model for predicting the ground-borne vibrations generated by a double-deck tunnel excited with a harmonic load. The results of the model are obtained coupling the interior floor and the tunnel-soil system in the wavenumber domain. The interior floor is modeled as an infinite thin plate (a strip plate) and the tunnel-soil system is modeled using the PiP model. The paper is structured as follows: In Section 2 the analytical formulation of the model is described. Section 3 is devoted to describe and solve the problems found in the numerical computation of the model. Section 4 discusses some results obtained for a particular set of mechanical parameters. Finally, Section 5 presents the conclusions drawn from the performed work.

2. Analytical formulation

The double-deck tunnel is modelled as an infinitely long circular cylindrical tunnel of constant thickness h_t and constant mean radius r_t divided in two halves by an interior floor of constant thickness h_p and no curvature. The tunnel is considered to be embedded in a full-space and, therefore, the effect of the surface is not taken into account. As has been shown in Hussein et al. (2006), the half-space response can be directly obtained from the full-space one. A cross-section of the model is presented in Fig. 1 where a harmonic point load is applied at a position of the interior floor (Point 4) and the resulting displacements are obtained at a position in soil (Point 3).

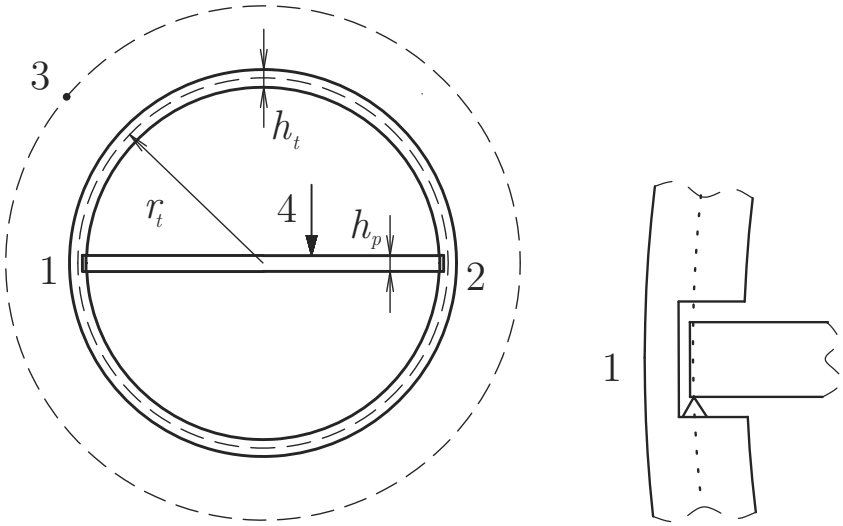

Fig. 1: (a) Cross-section of the double-deck circular tunnel model and (b) coupling hypothesis considered. The floor is supported at Points 1 and 2, the response is computed at Point 3 and the force is applied at Point 4.

Before formulating the model, two comments about the notation used for the displacement, force and stress variables are done. First, because the response to harmonic loads is studied, any dynamic variable f of the problem can be written as

$$\mathbf{f}(x,\dots,t) = \mathbf{F}(x,\dots)\mathrm{e}^{\mathrm{i}\omega t}, \tag{1}$$

where ω is frequency and t is time. Second, because the tunnel structure is assumed to be infinite and invariant in the train circulation direction (x-direction in the chosen system of coordinates), the dynamic variables are transformed to the wavenumber domain applying a Fourier transform of the following form

$$\bar{\mathbf{F}}(k_x,\dots) = \int_{-\infty}^{\infty} \mathbf{F}(x,\dots)\mathrm{e}^{\mathrm{i}k_x x}\mathrm{d}x, \tag{2}$$

where the bar notation is used to express that a variable is written in the transformed domain. Its corresponding inverse transform, which will be used for obtaining the results in the space domain, is

$$\mathbf{F}(x,\dots) = \frac{1}{2\pi}\int_{-\infty}^{\infty} \bar{\mathbf{F}}(k_x,\dots)\mathrm{e}^{-\mathrm{i}k_x x}\mathrm{d}k_x. \tag{3}$$

where k_x is the wavenumber in the transformed direction.

In the following subsections the analytical models developed for the interior floor of the tunnel and for the coupled double-deck tunnel-soil system are developed.

2.1. Interior floor model

The interior floor of the tunnel is represented as a homogeneous and isotropic thin plate of constant thickness h_p, constant width L_p and of infinite extent

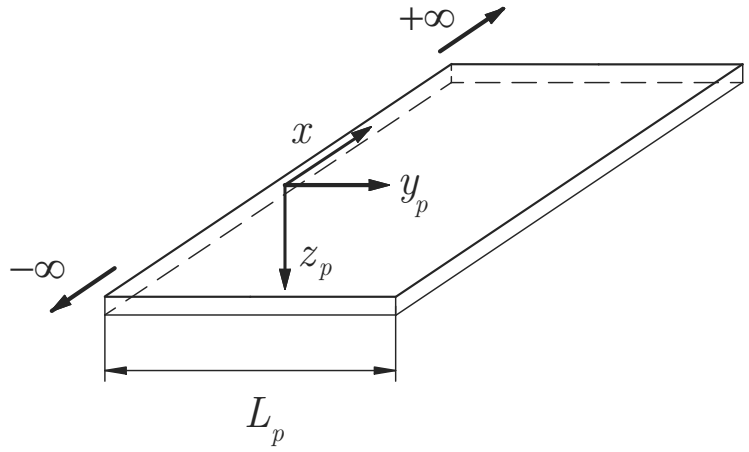

Fig. 2: Model and system of coordinates considered for the strip plate.

in the x-direction. This type of plate, represented in Fig. 2, will be referred as a strip plate in this work. A Cartesian system of coordinates (x, y_p, z_p) is chosen, where the subscript p, related to the plate, is not used for the x-coordinate because this coordinate is shared by both subsystems of the problem. The system is excited by a harmonic load with an arbitrary distribution $P(x)$ along the tunnel direction and applied at $y_p = y_j$. This type of load will be later used for describing both the external load and the interior floor-tunnel coupling forces. Under the considered conditions, the transverse equation of motion of a thin plate in a Cartesian system of coordinates takes the form

$$D_p \nabla^4 w_p(x, y_p, t) = P(x)\delta(y_p - y_j)\mathrm{e}^{\mathrm{i}\omega t} - \rho_p h_p \frac{\partial^2 w_p(x, y_p, t)}{\partial t^2}, \tag{4}$$

where

$$D_p = \frac{E_p h_p^3}{12(1 - \nu_p^2)} \tag{5}$$

is the flexural rigidity of the plate w_p is its deflection, ρ_p is its density, E_p is

its Young's modulus, ν_p is its Poisson's ratio, δ is the Dirac delta and

$$\nabla^4 = \frac{\partial^4}{\partial x^4} + 2\frac{\partial^4}{\partial x^2 \partial y_p^2} + \frac{\partial^4}{\partial y_p^4} \tag{6}$$

is the biharmonic operator.

Assuming harmonic motion and applying a Fourier transform of the form defined in Eq. (2), Eq. (4) becomes

$$\left(\frac{\mathrm{d}^4}{\mathrm{d}y_p^4} - 2k_x^2\frac{\mathrm{d}^2}{\mathrm{d}y_p^2} + (k_x^4 - \kappa^4)\right)\bar{W}_p(y_p) = \frac{\bar{P}\delta(y_p - y_j)}{D_p}, \tag{7}$$

where

$$\kappa = \left(\frac{\rho_p h_p \omega^2}{D_p}\right)^{1/4}. \tag{8}$$

To obtain the free response of the system, proper boundary conditions at both edges of the finite dimension of the plate have to be considered. Because the double-deck tunnel response will be obtained using the method of coupling subsystems, the free response of these subsystems is required. The well-known free edge boundary conditions (detailed, for example, in Graff (1975)) are transformed to the wavenumber domain obtaining

$$\begin{aligned} \left(\frac{\mathrm{d}^3\bar{W}_p}{\mathrm{d}y_p^3} - (2-\nu_p)k_x^2\frac{\mathrm{d}\bar{W}_p}{\mathrm{d}y_p}\right)\Bigg|_{y_p=0,L_p} &= 0, \\ \left(\frac{\mathrm{d}^2\bar{W}_p}{\mathrm{d}y_p^2} - \nu_p k_x^2\bar{W}_p\right)\Bigg|_{y_p=0,L_p} &= 0. \end{aligned} \tag{9}$$

Eq. (7) with the boundary conditions defined in Eq. (9) has two kinds of nontrivial solutions. For $\kappa^2 > k_x^2$ the following characteristic equation is obtained

$$\begin{aligned} &2\zeta_1\zeta_2\gamma_1^2\gamma_2^2[\cosh(\zeta_1 L_p)\cos(\zeta_2 L_p) - 1] = \\ &\sinh(\zeta_1 L_p)\sin(\zeta_2 L_p)[\zeta_1^2\gamma_2^4 - \zeta_2^2\gamma_1^4], \end{aligned} \tag{10}$$

where $\zeta_1 = \sqrt{\kappa^2 + k_x^2}$, $\zeta_2 = \sqrt{\kappa^2 - k_x^2}$, $\gamma_1 = \kappa^2 + k_x^2(1 - \nu_p)$ and $\gamma_2 = \kappa^2 - k_x^2(1 - \nu_p)$.

For $\kappa^2 < k_x^2$, the characteristic equation is

$$\begin{aligned} &2\zeta_1\zeta_2^{'}\gamma_1^2\gamma_2^2[\cosh(\zeta_1 L_p)\cosh(\zeta_2^{'} L_p) - 1] = \\ &\sinh(\zeta_1 L_p)\sinh(\zeta_2^{'} L_p)[\zeta_1^2\gamma_2^4 + \zeta_2^{'2}\gamma_1^4], \end{aligned} \tag{11}$$

where $\zeta_2^{'2} = -\zeta_2^2$.

For any value of k_x considered, a discrete infinite set of eigenfrequencies ω_n are obtained from the roots of Eq. (10). Also, as it is mathematically demonstrated in Leissa (1993), because Eq. (11) always has one root, an additional eigenfrequency has to be added to the previous set. The work of Leissa also demonstrates that a second root is obtained under certain restrictive conditions. However, due to its infinite length, these conditions cannot be met by a strip load.

The corresponding eigenfunction $\bar{W}_n(y_p)$ of each root found for $\kappa^2 > k_x^2$ can be written as

$$\begin{aligned} \bar{W}_n(y_p) \;=\; &\zeta_2\gamma_1\sinh(\zeta_1 y_p) + \zeta_1\gamma_2\sin(\zeta_2 y_p) \\ &-\sigma_{FF}[\gamma_2\cosh(\zeta_1 y_p) + \gamma_1\cos(\zeta_2 y_p)], \end{aligned} \tag{12}$$

where

$$\sigma_{FF} = \frac{\zeta_2\gamma_1^2 \sinh(\zeta_1 L_p) - \zeta_1\gamma_2^2 \sin(\zeta_2 L_p)}{\gamma_1\gamma_2[\cosh(\zeta_1 L_p) - \cos(\zeta_2 L_p)]}. \tag{13}$$

For the root found for $\kappa^2 < k_x^2$ its corresponding eigenfunction $\bar{W}_n(y_p)$ can be written as

$$\begin{aligned} \bar{W}_n(y_p) &= \zeta_2^{'}\gamma_1 \sinh(\zeta_1 y_p) + \zeta_1\gamma_2 \sinh(\zeta_2^{'} y_p) \\ &\quad -\sigma_{FF}^{'}[\gamma_2 \cosh(\zeta_1 y_p) + \gamma_1 \cosh(\zeta_2^{'} y_p)], \end{aligned} \tag{14}$$

where

$$\sigma_{FF}^{'} = \frac{\zeta_2^{'}\gamma_1^2 \sinh(\zeta_1 L_p) - \zeta_1\gamma_2^2 \sinh(\zeta_2^{'} L_p)}{\gamma_1\gamma_2[\cosh(\zeta_1 L_p) - \cosh(\zeta_2^{'} L_p)]}. \tag{15}$$

The forced response of the strip plate in the wavenumber domain is obtained by the modal superposition method. This response is given by

$$\bar{W}_p(y_p) = \sum_{n=1}^{\infty} \frac{\bar{W}_n(y_p) p_n}{D_p(\kappa_n^4 - \kappa^4)}, \tag{16}$$

where

$$\kappa_n = \left(\frac{\rho_p h_p \omega_n^2}{D_p} \right)^{1/4}. \tag{17}$$

For the type of loads considered, the coefficients p_n are given by

$$p_n = \frac{1}{C_n}\int_0^{L_p} \bar{P}\delta(y_p - y_j)\bar{W}_n(y_p)\mathrm{d}y_p = \frac{\bar{P}\bar{W}_n(y_j)}{C_n}, \tag{18}$$

where

$$C_n = \int_0^{L_p} \bar{W}_n(y_p)^2\mathrm{d}y_p. \tag{19}$$

It is assumed that the volumetric and deviatoric structural damping ratios of the interior floor are equal. Therefore, damping is introduced in the model by defining a complex Young's modulus of the form

$$E_p^* = E_p(1 + \mathrm{i}\eta_p), \tag{20}$$

where η_p is the loss factor of the interior floor (see, for example, Söedel (1993)). Substituting Eqs. (8), (17) and (20) into (16), the forced response can be written as

$$\bar{W}_p(y_p) = \sum_{n=1}^{\infty} \frac{\bar{W}_n(y_p)p_n}{\omega_n^2\rho_p h_p\left((1 + \mathrm{i}\eta_p) - \dfrac{\omega^2}{\omega_n^2}\right)}. \tag{21}$$

The receptance of the plate in the wavenumber domain is finally obtained substituting Eq. (18) into Eq. (21). The receptance $\bar{\alpha}_{ij}$ at a position $y_p = y_i$ due to a force $\bar{P}$ applied at $y_p = y_j$ can be written as

$$\bar{\alpha}_{ij} = \frac{\bar{W}_p(y_i)}{\bar{P}} = \sum_{n=1}^{\infty} \frac{\bar{W}_n(y_i)\bar{W}_n(y_f)\mathrm{e}^{\mathrm{i}\phi_n}}{C_n\rho_p h_p\sqrt{(\omega_n^2 - \omega^2)^2 + \omega_n^4\eta_p^2}}, \tag{22}$$

where

$$\phi_n = \arctan\left(\frac{\eta_p}{1-(\omega/\omega_n)^2}\right). \tag{23}$$

The plate receptance will be later used for obtaining the interior floor-tunnel coupling forces.

2.2. Double-deck tunnel model

The soil and the tunnel dynamics are described using the PiP model derived in Forrest and Hunt (2006b). In their work, the tunnel is assumed to behave as a thin cylindrical shell and the soil is modeled as an infinite linear isotropic homogeneous elastic media. The coupling between both systems is performed in the frequency-wavenumber domain considering equal displacement fields and opposite stress fields at the interface. The positive directions considered for the displacements (u_x, u_θ and u_r) and for the stresses (τ_{rx}, $\tau_{r\theta}$ and τ_{rr}) and the considered system of coordinates (x, θ, r) are presented in Fig. 3. The PiP formulation will be directly used in this work but the interested reader can find a complete derivation of the expressions and details regarding its numerical computation in Forrest and Hunt (2006b) and Hussein and Hunt (2007).

As it is detailed in Section 4, the interior floor-tunnel coupling forces are assumed to be tangential forces applied at angular positions $\theta = 0$ and $\theta = \pi$, respectively. With the chosen origin of the angular coordinate, both loads can be decomposed using only the antisymmetric PiP model formulation, which was developed in Hussein and Hunt (2007). This axis definition not only simplifies the complexity of the analytic formulation but also improves the computational efficiency of the model. Once applied, the response of the tunnel-soil system in the wavenumber-frequency domain is given by

$$\begin{pmatrix} \bar{U}_x \\ \bar{U}_\theta \\ \bar{U}_r \end{pmatrix} = \sum_{n=0}^{\infty} \begin{pmatrix} \sin n\theta & 0 & 0 \\ 0 & \cos n\theta & 0 \\ 0 & 0 & \sin n\theta \end{pmatrix} \begin{pmatrix} \bar{U}_{x,n} \\ \bar{U}_{\theta,n} \\ \bar{U}_{r,n} \end{pmatrix}. \tag{24}$$

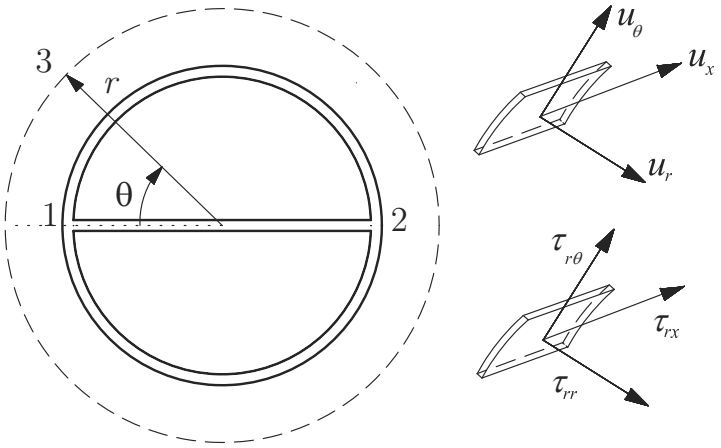

Fig. 3: Cross-section of the double-deck circular tunnel model with the chosen system of coordinates and the positive directions considered for the displacement and stress fields.

The ring modes coefficients of the displacement field are obtained from

$$\bar{\mathbf{U}}_n = \left[\mathbf{U}\Big|_{r_m} (\mathbf{A_E}\mathbf{U}\Big|_{r_t} + \mathbf{T}\Big|_{r_t})^{-1} \right] \bar{\mathbf{P}}_n = \mathbf{H}\bar{\mathbf{P}}_n, \tag{25}$$

where the coefficients $\bar{\mathbf{P}}_n$ are obtained from the ring modes decomposition of the applied antisymmetric load and where the definitions of the matrices $\mathbf{A_E}$, $\mathbf{U}$ and $\mathbf{T}$ are presented in the Appendix A.

The response of the double-deck tunnel is obtained coupling the two comprising subsystems: the interior floor subsystem and the coupled tunnel-soil subsystem. For modelling this coupling it has been considered that the edges of the interior floor are supported by the tunnel wall (Points 1 and 2 in Fig. 1). This assumption is a realistic simplification for the cases where the interior floor has been constructed as a precast slab, which is the case, for example, of Barcelona metro Line 9. Assuming, because the external loads have no horizontal components, that the inplane response of the thin plate is negligible compared to its transverse response, the interaction between both systems is completely defined by two x-distributed coupling forces. While in the case of the interior floor coordinates the coupling forces are represented as

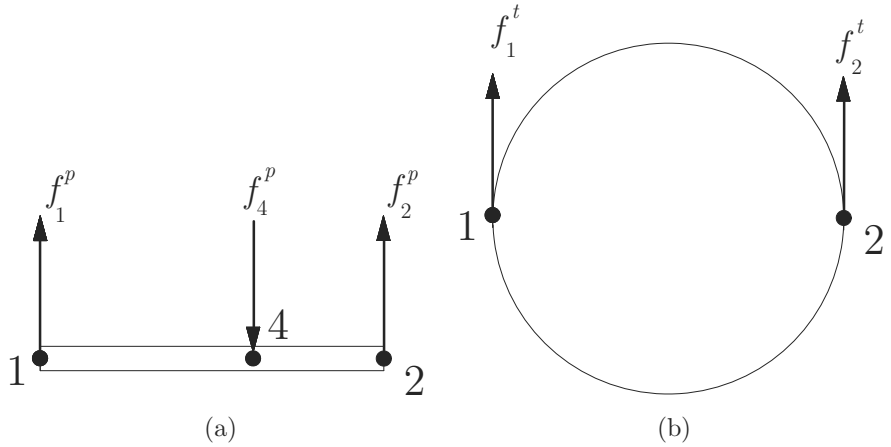

Fig. 4: (a) Free body diagram of the interior floor (b) Free body diagram of the tunnel-soil system.

transversal forces, for the tunnel-soil case they are tangential forces. The free body diagrams of both systems are the ones presented in Fig. 4. Note that an external force is also applied at Point 4 and that, because the coupling of the subsystems is performed in the wavenumber domain, the x-direction distribution of the loads is properly taken into account but has not been represented in this figure.

With this assumptions, the deflection of the plate in the wavenumber domain is given by

$$\bar{W}_p(y_i) = -\bar{\alpha}_{i1}\bar{F}_1^p - \bar{\alpha}_{i2}\bar{F}_2^p + \bar{\alpha}_{i4}\bar{F}_4^p, \tag{26}$$

where $\bar{F}_1^p$, $\bar{F}_2^p$ and $\bar{F}_4^p$ are the transformed external and unknown coupling loads.

In the same domain, the displacement field of the tunnel-soil is given by

$$\bar{\mathbf{U}} = \bar{\boldsymbol{\beta}}_{i,1}\bar{\mathbf{F}}_1^t - \bar{\boldsymbol{\beta}}_{i,2}\bar{\mathbf{F}}_2^t. \tag{27}$$

where $\bar{F}_1^t$, $\bar{F}_2^t$ are the unknown coupling loads acting on the tunnel and where $\bar{\boldsymbol{\beta}}_{i,1}$ and $\bar{\boldsymbol{\beta}}_{i,2}$ are the PiP wavenumber receptances, which are 3×3 matrices.

The considered coupling conditions between the strip plate and the PiP subsystems are

$$\begin{aligned} \bar{W}_p(0) &= -\bar{U}_{1\theta}, \qquad \bar{F}_1^p = -\bar{F}_1^t, \\ \bar{W}_p(L_p) &= \bar{U}_{2\theta}, \qquad \bar{F}_2^p = -\bar{F}_2^t, \end{aligned} \tag{28}$$

where the strip plate displacement are obtained using Eq. (26) and where the tangential displacements of the tunnel are obtained from Eq. (27). Because the applied forces on the tunnel are tangential forces and because the tangential displacement is the one required, only one element of the PiP receptance matrix in needed to describe the coupling. This element has been named $\bar{\beta}_{i\theta,j\theta}$ in the next equations. Applying the mentioned expressions in Eq. (28), the following system of equations is obtained

$$\begin{pmatrix} -(\bar{\alpha}_{11} + \bar{\beta}_{1\theta,1\theta}) & -\bar{\alpha}_{12} + \bar{\beta}_{1\theta,2\theta} \\ -\bar{\alpha}_{21} + \bar{\beta}_{2\theta,1\theta} & -(\bar{\alpha}_{22} + \bar{\beta}_{2\theta,2\theta}) \end{pmatrix} \begin{pmatrix} \bar{F}_1^t \\ \bar{F}_2^t \end{pmatrix} = \begin{pmatrix} \bar{\alpha}_{14} \\ \bar{\alpha}_{24} \end{pmatrix} \bar{F}_4^p. \tag{29}$$

While the plate receptances $\bar{\alpha}_{i,j}$ are directly obtained using Eq. (22), the PiP receptances are obtained from Eq. (24), which requires to know the tangential component of the force coefficients $\bar{\mathbf{P}}_n$. These are obtained from the coupling forces acting on the tunnel which, written in the space domain, take the following form

$$\mathbf{p}_1 = \begin{pmatrix} 0 \\ P_{1\theta}(x) \\ 0 \end{pmatrix} \frac{\delta(\theta)}{r_t} \mathrm{e}^{\mathrm{i}\omega t}, \qquad \mathbf{p}_2 = \begin{pmatrix} 0 \\ P_{2\theta}(x) \\ 0 \end{pmatrix} \frac{\delta(\theta - \pi)}{r_t} \mathrm{e}^{\mathrm{i}\omega t}. \tag{30}$$

The force coefficients are obtained omitting the harmonic dependance, transforming the space distributions to the wavenumber domain and performing a Fourier series decomposition of the Dirac delta functions. The resulting

expressions are

$$\begin{aligned} \bar{P}_{1\theta,0} &= \frac{1}{2r_t\pi}\bar{P}_{1\theta}, \qquad \bar{P}_{1\theta,n} = \frac{1}{r_t\pi}\bar{P}_{1\theta} \quad n>0, \\ \bar{P}_{2\theta,0} &= \frac{1}{2r_t\pi}\bar{P}_{2\theta} \qquad \bar{P}_{2\theta,n} = \frac{(-1)^n}{r_t\pi}\bar{P}_{2\theta} \quad n>0. \end{aligned} \tag{31}$$

Substituting Eq. (31) into the tangential component of Eq. (24), the PiP receptances can be written as

$$\begin{aligned} \bar{\beta}_{1\theta,1\theta} &= \frac{h_{22,0}}{2r_t\pi} + \frac{1}{r_t\pi}\sum_{n=1}^{\infty} h_{22,n}, \\ \bar{\beta}_{1\theta,2\theta} &= \frac{h_{22,0}}{2r_t\pi} + \frac{1}{r_t\pi}\sum_{n=1}^{\infty} h_{22,n}(-1)^n, \end{aligned} \tag{32}$$

where $h_{22,(0/n)}$ is the $(0/n)$-th term of this element of $\mathbf{H}$.

In obtaining the coupling forces some numerical calculations can be avoided if the Maxwell reciprocity principle is used, which ensures that $\bar{\alpha}_{ij} = \bar{\alpha}_{ji}$ and $\bar{\boldsymbol{\beta}}_{i,j} = \bar{\boldsymbol{\beta}}_{j,i}$. Once the coupling forces are calculated, the displacement fields of each subsystem in the wavenumber domain are obtained from Eqs. (26) and (27). The response of the system in the space domain is finally obtained applying Eq. (3).

3. Numerical computation

The computation of the model requires to deal properly with two numerical issues: the correct evaluation of any ill-behaved analytic expression used and the correct evaluation of the numerical inverse Fourier transform performed to obtain the response in the space domain. The following subsections propose alternative well-behaved expressions for the plate eigenfunctions and discuss how the Fourier transforms, the matrix inversions and the modal summations should be done to ensure good accuracy in the results.

3.1. Eigenfunctions correction

The strip plate eigenfunctions presented in Eqs. (12) and (14) are numerically ill-behaved expressions. These solutions are not stable for large arguments of the hyperbolic functions appearing in them, becoming necessary to perform some analytical modifications in order to obtain accurate results. For the case of beam eigenfunctions, a procedure to overcome similar numerical problems has been presented by Gonçalves et al. (2007). This procedure is applied here to the strip plate eigenfunctions.

Dividing Eq. (12) by $\zeta_2\gamma_1$ and using that $\sinh(\zeta_1 y_p) - \cosh(\zeta_1 y_p) = -\mathrm{e}^{-\zeta_1 y_p}$, the eigenfunction can be expressed as

$$\bar{W}_n(y_p) = -\mathrm{e}^{-\zeta_1 y_p} + \nu_{FF}\cosh(\zeta_1 y_p) + \frac{\zeta_1\gamma_2}{\zeta_2\gamma_1}\sin(\zeta_2 y_p) - \frac{\sigma_{FF}}{\zeta_2}\cos(\zeta_2 y_p), \quad (33)$$

where

$$\nu_{FF} = 1 - \frac{\sigma_r\gamma_2}{\zeta_2\gamma_1}.$$

The numerical instability of the strip plate eigenmodes is easy to understand analysing Eq. (33). For high values of $\zeta_1 L_p$, the term ν_{FF} becomes smaller than the floating-point relative accuracy typically used by numerical softwares. When this occurs, the product $\nu_{FF}\cosh(\zeta_1 y_p)$, despite having a significant contribution to the eigenfunction value, is numerically equal to zero. Due to this, the numerical calculation of the eigenmode amplitude is inaccurate.

This problem has been solved in this work in the following way (Gonçalves et al. (2007)). For large values of ζ_1, $\cosh(\zeta_1 L_p) >> \cos(\zeta_2 L_p)$, and the instable term can be approximated as follows

$$\begin{aligned}\nu_{FF}\cosh(\zeta_1 y_p) &= [\frac{\gamma_1^2 z_2 \mathrm{e}^{-\zeta_1 L_p} + \zeta_1\gamma_2^2\sin(\zeta_2 L_p) - \zeta_2\gamma_1^2\cos(\zeta_2 L_p)}{\gamma_1^2\zeta_2[\cosh(\zeta_1 L_p) - \cos(\zeta_2 L_p)]}]\cosh(\zeta_1 y_p) \\ &\approx \frac{\cosh(\zeta_1 y_p)}{\cosh(\zeta_1 L_p)}[\mathrm{e}^{-\zeta_1 L_p} + \frac{\zeta_1\gamma_2^2}{\zeta_2\gamma_1^2}\sin(\zeta_2 L_p) - \cos(\zeta_2 L_p)].\end{aligned}$$

Then, using that

$$\frac{\cosh(\zeta_1 y_p)}{\cosh(\zeta_1 L_p)} \approx \mathrm{e}^{\zeta_1(y_p - L_p)} + \mathrm{e}^{-\zeta_1(y_p + L_p)},$$

the term can be finally written as

$$\nu_{FF}\cosh(\zeta_1 y_p) \approx [\mathrm{e}^{\zeta_1(y_p - L_p)} + \mathrm{e}^{-\zeta_1(y_p + L_p)}]\left[\frac{\zeta_1\gamma_2^2}{\zeta_2\gamma_1^2}\sin(\zeta_2 L_p) - \cos(\zeta_2 L_p)\right].$$

which is no longer a numerically ill-behaved expression. The same procedure has been applied to Eq. (14).

3.2. Samplings and truncations

The response of the system in the space domain is obtained using the inverse Fourier transform defined in Eq. (3). Because this transform cannot be performed analytically, numerical integration techniques have to be applied. When results are desired in different cross-sections, the most efficient way to perform this integration is to use the computational efficiency of the Fast Fourier Transform (FFT) algorithm. In contrast, if results are only required in a small number of cross-sections, higher accuracy is obtained using other numerical integration methods such as an adaptative quadrature (Shampine (2008)). In both cases, the numerical computation of the inverse transforms has been performed considering an equispaced sampling of the corresponding

integrands. This sampling is completely defined by the number of samples N and the sampling resolution Δk.

The numerical computation of the modal summations presented in Eqs. (22) and (32) has to be truncated taking into account the frequency range of interest in ground-borne vibrations. For underground vibrations this range is 1-80 Hz (ISO 14837-1:2005) but results are sometimes presented up to 200 Hz, the range of frequencies where the reradiated noise is significant. In order to obtain accurate results, it is expected that modes with eigenfrequencies far over the upper limit of the frequency range of interest will not have a significant contribution to the response. This conclusion is later tested in the results section, where a convergence test is performed.

The last comment is related to the matrices inverted in Eq. (25), which are ill-conditioned matrices. To avoid the numerical problems found in their inversion, a **LU** decomposition has been used.

4. Results and discussion

This section presents and discusses the results obtained using the developed model. The first subsection is devoted to understand the response of the strip plate subsystem and the second one presents results regarding the dynamical behavior of a double-deck tunnel.

4.1. Interior floor results

To ensure that the analytical model of the strip plate has been correctly formulated and computed, its response to an external load has been compared to the one obtained using a numerical model of this system. This numerical model has been developed using the 2.5D FE formulation used in François et al. (2010). The cross-section of the strip plate has been meshed using 6976 linear triangular elements. The chosen mechanical parameters of the interior floor are detailed in Table 1.

Fig. 5 presents a comparison between the response of both models for three

Table 1: Mechanical parameters used to model the interior floor as a strip plate.

Parameter	Value
L_p	10.9 m
h_p	0.4 m
E_p	27.6 GPa
ν_p	0.175
ρ_p	3000 kg m^{-3}
η_p	0.02

different wavenumbers: $k_x = 0,\ \pi/16$ and $\pi/2$ rad $\cdot$ m^{-1}. Very good agreement is obtained for all the frequency range 1-80 Hz. Significant differences have been only observed for frequencies beyond this range, where higher order elements or a larger number of them may be necessary. The results have been obtained considering a vertical point load applied at $(x, y_p) = (0, 5.45)$ m and comparing the vertical response at $y_p = 3.3$ m. In the FE model the considered node is situated at the upper surface of the strip plate.

Applying Eq. (3) the results obtained with both models have been transformed to the space domain. In Fig. 6 the results of this transformation are compared for three different axial distances: $x_m = 0$, 10 and 25 m (see Fig. 2). Again, very small differences have been found between them for the range of frequencies of interest. Because of the relation between the space and the wavenumber results, this comparison ensures that a very good agreement has been obtained for all the wavenumber values considered.

The strip plate response presented in Fig. 5 shows some sharp peaks at frequencies that depend on the considered wavenumber. This phenomena can be properly explained observing the dispersion curves of the strip plate, which can be obtained computing the roots of Eqs. (10) and (11). For the mechanical parameters considered, these curves are presented in Fig. 7. Several propagating wave modes are possible for each wavenumber. Because these modes are y_p-symmetric or y_p-antisymmetric, only those compatible both with the load and with the response positions contribute to the strip plate displacement. Therefore, due to the position where the external load has been applied, the response shown in Fig. 5 is exclusively formed from the contribution of symmetric modes.

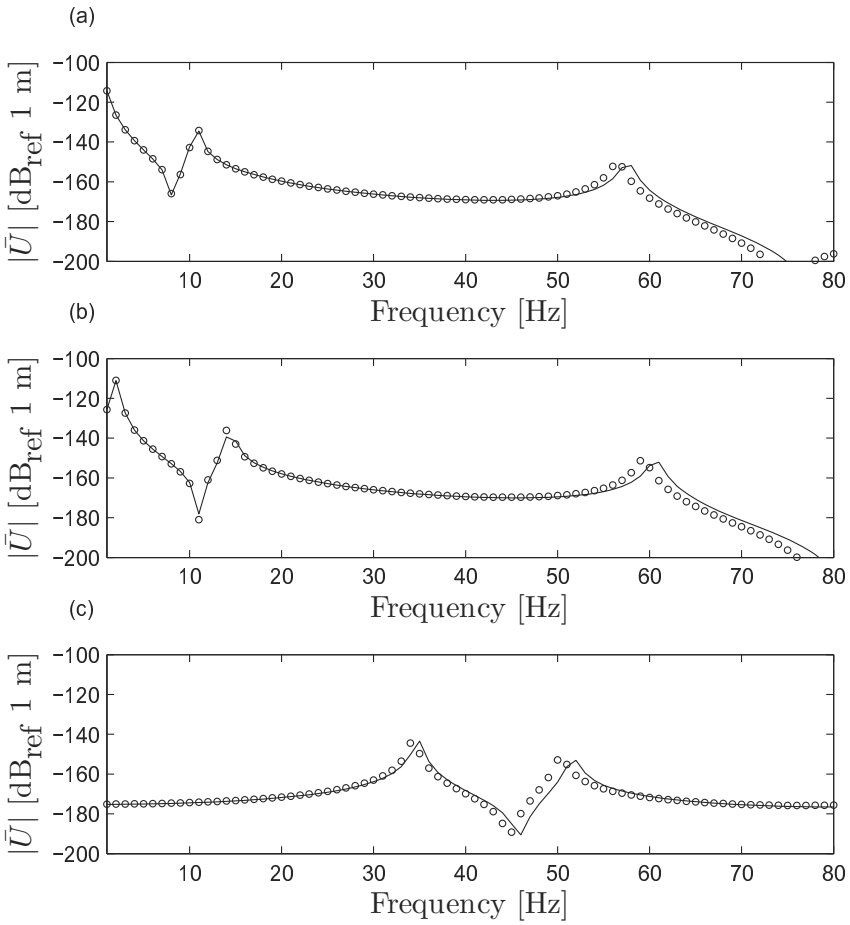

Fig. 5: Comparison of the strip plate displacements $\bar{U}$ for the case of the analytic (line) and the numerical model (circles). Results are presented at wavenumbers: (a) $k_x = 0$ rad$\cdot$m^{-1}, (b) $k_x = \pi/16$ rad $\cdot$ m^{-1} and (c) $k_x = \pi/2$ rad $\cdot$ m^{-1}.

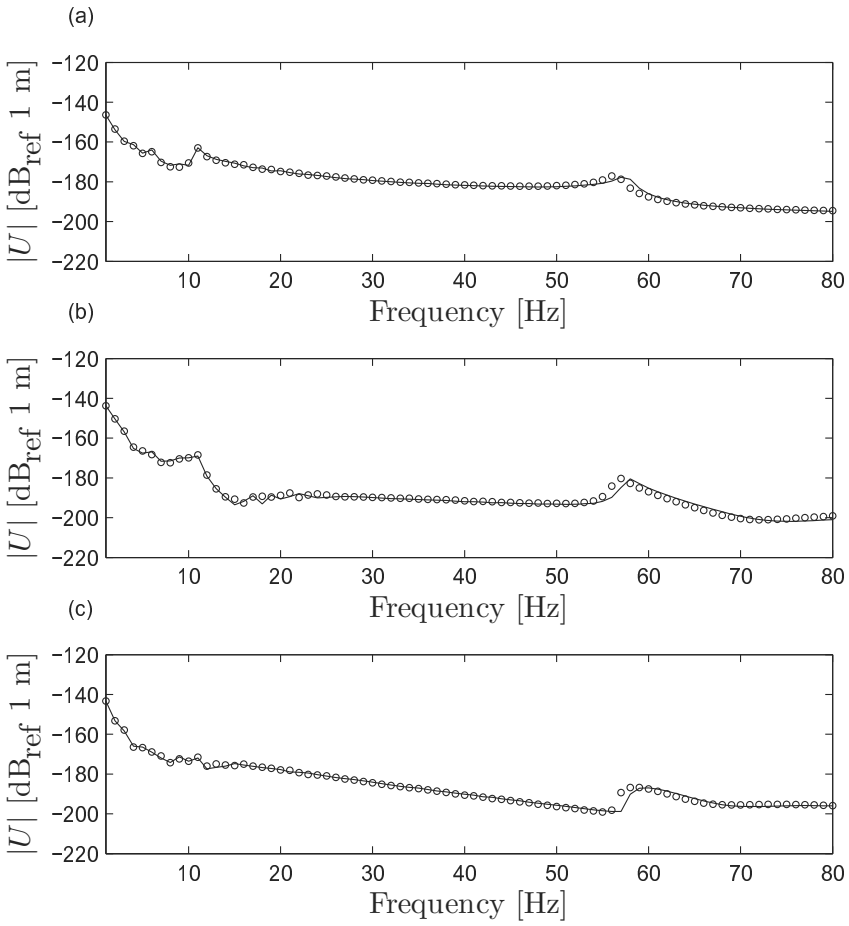

Fig. 6: Comparison of the strip plate response U to a unit point load for the case of the analytic (line) and the numerical model (circles). Results are presented for different cross-sections: (a) $x_m = 0$ m, (b) $x_m = 10$ m and (c) $x_m = 25$ m.

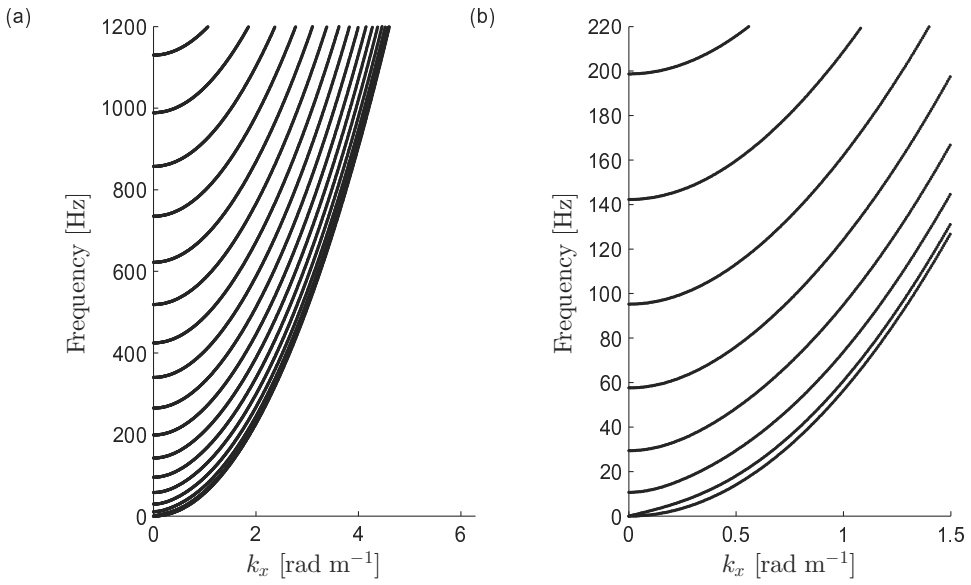

Fig. 7: Dispersion curves of the strip plate. (a) Up to 1200 Hz (b) Up to 220 Hz.

As has been mentioned in the previous section, the infinite summation of modes in Eq. (22) is limited to the modes existing up to a truncation frequency f_t. From Fig. 7 it is clear that the number of modes contributing to the strip plate response for a given truncation frequency decreases as the value of the wavenumber increases. In particular, for any truncation frequency considered, there is a limit value of the wavenumber over which no modes are found and the response of the strip plate , which is computed using the modal superposition method, is numerically equal to zero.

4.2. Double-deck tunnel results

The correct computation of the soil response requires to consider adequate values for the following parameters: The wavenumber resolution Δk_x, the number of samples considered N, the number of ring modes and the number of strip plate modes. The criteria used for the first three parameters is the one presented in Forrest and Hunt (2006b). Convergence tests for them are not presented here but the interested reader can find them in Clot (2014), where it is shown that very good results are obtained considering $N = 2048$

Table 2: Mechanical parameters used to model the tunnel as a thin cylindrical shell.

Parameter	Value
r_t	5.65 m
h_t	0.4 m
E_t	27.6 GPa
ν_t	0.175
ρ_t	3000 kg m^{-3}
D_{E_t}	0.02

samples, $\Delta k_x = \pi/512$ rad $\cdot$ m^{-1} and 15 ring modes. These values have been used in all the results presented in this section.

The convergence tests have been performed calculating the maximum displacement magnitude u_{m} of the soil. This is given by

$$u_{\mathrm{m}}^2 = \sum_{i=1}^{3} \frac{|U_i|^2}{2} + \sqrt{\mathfrak{s}^2 + \mathfrak{c}^2}, \tag{34}$$

where

$$\mathfrak{s} = \sum_{i=1}^{3} \frac{|U_i|^2}{2} \sin(2\phi_i), \qquad \mathfrak{c} = \sum_{i=1}^{3} \frac{|U_i|^2}{2} \cos(2\phi_i), \tag{35}$$

where $\phi_i = \mathrm{Im}(U_i)/\mathrm{Re}(U_i)$ and U_i the i-th component of the soil displacement.

Fig. 8 presents the convergence test performed to obtain an adequate truncation frequency. The maximum displacement magnitude caused by a vertical point load applied at $(x, y_p) = (0, 5.45)$ m is presented for the frequency range 1-200 Hz with a frequency resolution of $\Delta f = 1$ Hz. The results are obtained at $\theta_m = \pi/3$ rad and $r_m = 10$ m for three different axial distances: $x = 0$, 10 and 25 m. The mechanical parameters considered for the interior floor, for the tunnel and for the soil are detailed in Tables 1, 2 and 3 respectively. They are typical values of a reinforced concrete and of a soft tertiary ground.

The results show that, for the range of frequencies considered, small differences are found between the three truncation frequencies considered. Therefore, the response of the double-deck tunnel can be accurately computed

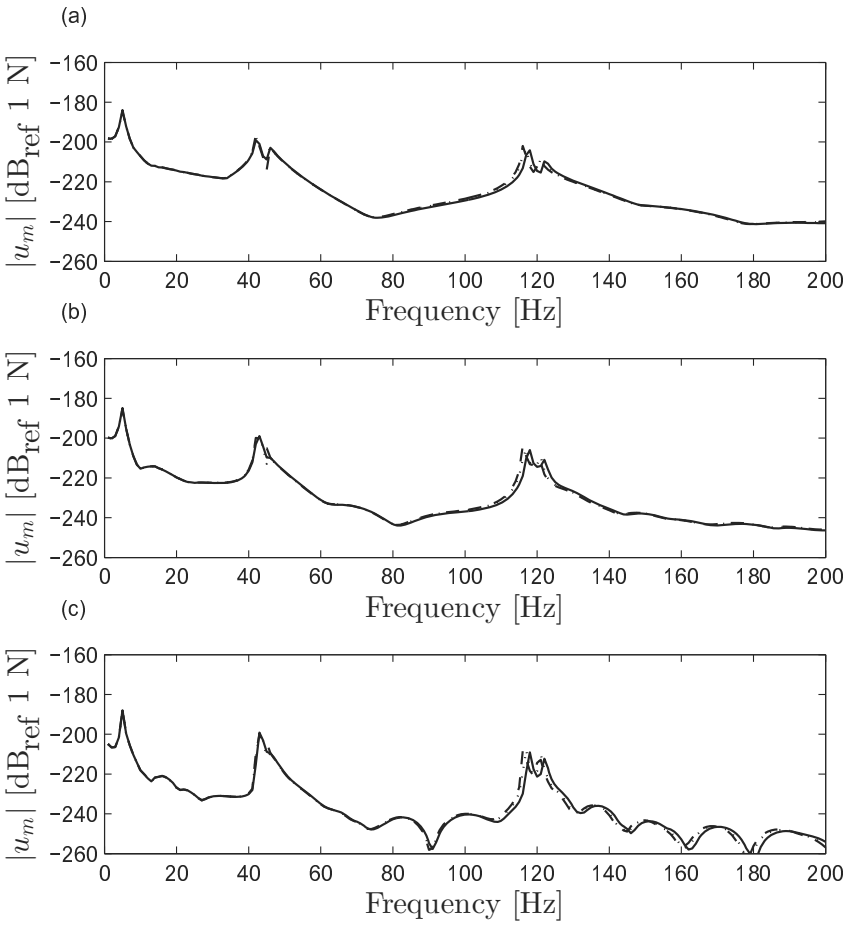

Fig. 8: Maximum displacement magnitude of a double-deck tunnel considering $f_t = 400$ Hz (continuous), 800 Hz (dotted) and 3200 Hz (dashed). The cross-sections considered are: (a) $x_m = 0$ m, (b) $x_m = 10$ m, (c) $x_m = 25$ m.

Table 3: Mechanical parameters used to model the soil as an elastic continuum.

Parameter	Value
E_s	100 MPa
ν_s	0.3
ρ_s	1950 kg m^{-3}
D_P	0.03
D_S	0.03

considering a truncation value of 400 Hz.

The results presented in Fig. 8 also show that the soil response to a harmonic point load applied on the strip plate show significant peaks around 5, 40 and 120 Hz. These peaks arise around the same frequencies for all the cross-sections considered being related to the propagation of long wavelengths or small wavenumbers. For a better understanding of their origin, the strip plate-tunnel coupling loads will be firstly quantified.

Fig. 9 presents the magnitude of the coupling load $\bar{F}_1^p$ for three different frequencies: 20, 50 and 150 Hz. The results have been obtained computing Eq. (29) for a harmonic unitary vertical point load at $(x, y_p) = (0, 5.45)$ m. Because the external load is applied at the same distance of both strip plate edges, the coupling loads are equal. This symmetry has been tested to ensure the correctness of the results. The coupling loads have been obtained for the three different truncation frequencies considered before.

The results show that the magnitude of the coupling loads depends significantly on the considered wavenumber and excitation frequency. As the frequency increases, both the number of peaks of amplitude found and the wavenumber where these peaks occur also increases. The wavenumber-frequency values where the peaks appear has a very good agreement with the results presented in Fig. 7. This can be easily explained looking at Eq. (29). Once the matrix of receptances is inverted, the coupling loads are the result of multiplying this inverse by the strip plate receptace of each edge. High values of the coupling loads will be obtained when one or both of these terms exhibits a peak of response. While for the inverse of receptances this requires a proper combination of the strip plate and the PiP receptances,

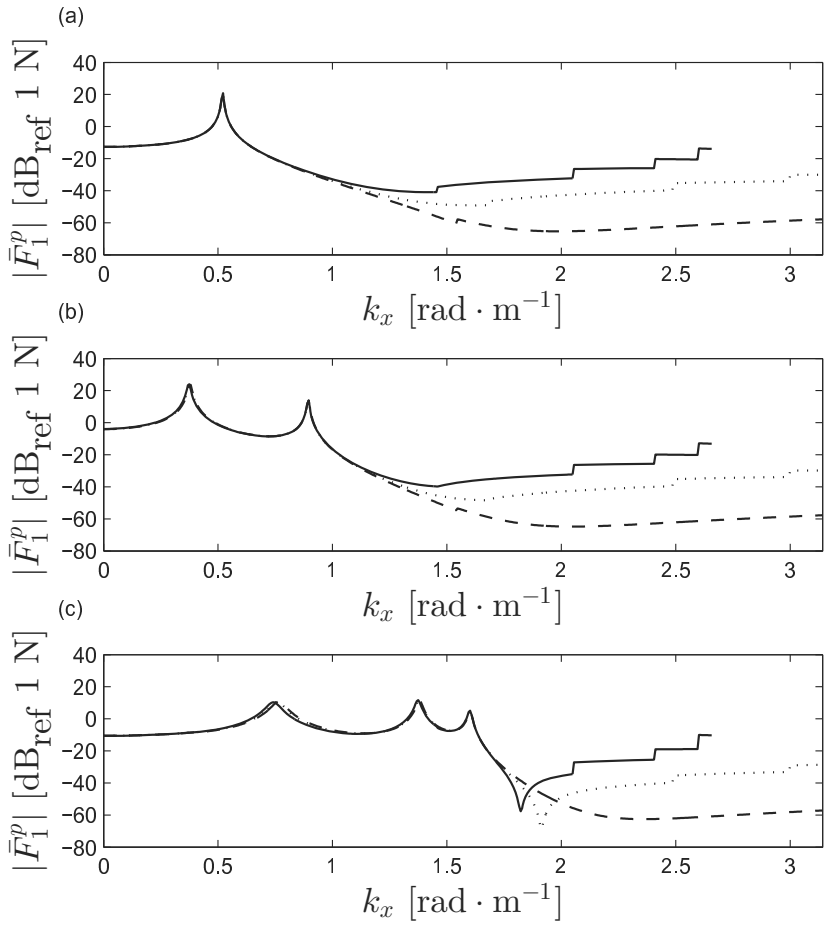

Fig. 9: Magnitude of the coupling load $\bar{F}_1^p$ considering $f_t = 400$ Hz (continuous), 800 Hz (dotted) and 3200 Hz (dashed). The excitation frequencies considered are: (a) 20 Hz, (b) 50 Hz and (c) 150 Hz.

for the second term this peaks of response are obtained when the strip plate presents a wave propagation mode. The results show that it is this second term that governs the magnitude of the coupling loads between the tunnel wall and the interior floor.

Fig. 9 also shows that, for high wavenumbers, important differences in the magnitude of the coupling forces are found when the truncation frequency is increased. These differences can be explained looking again at the dispersion curves of the strip plate. For any truncation frequency considered, the higher the wavenumber value is the smaller the number of modes contributing to the strip plate becomes. The consequence of this reduction is that the accuracy of the calculation performed decreases and that the coupling loads amplitude is not calculated properly. In particular, for a truncation frequency of 400 Hz, no modes are found for wavenumbers over approximately 2.6 rad $\cdot$ m^{-1}, and the coupling load is numerically equal to 0. It may seem that a very large truncation frequency is needed for obtaining good results but, as has been previously presented in Fig. 8, accurate results are obtained considering 400 Hz. This can be easily understood noting that, in the frequency-wavenumber domain, the response of the soil, given by Eq. (27), is obtained from the product of the coupling forces by the PiP model receptances. In the considered frequency range of interest, the PiP response is very small at high wavenumbers and, even if the applied load has a significant amplitude at these values, the response of the double-deck system is negligible. Due to this, the soil response is correctly computed with a relatively small truncation frequency, as has been previously shown.

Fig. 10 presents a comparison between the responses of a double-deck tunnel and of a simple tunnel. The comparison is performed comparing both the maximum displacement magnitudes at a certain point of the soil. The chosen point is situated at $r_m = 10$ m over the tunnel apex ($\theta_m = \pi/2$ in the double-deck model system of coordinates and $\theta_m = \pi$ in the PiP one). The comparison has been performed applying a vertical point load at $y_p = 5.45$ m at the interior floor of the double-deck tunnel and a radial point load at the tunnel invert of the simple tunnel. The correctness of the PiP computation has been tested reproducing all the tunnel-soil results presented in Gupta et al. (2007). Because this work uses the thick shell formulation of the PiP model instead of the thin shell one, the results obtained using both have been also compared. Very small differences have been found for the mechanical

parameters considered in this work.

Two main differences can be observed in the comparison of both responses. The first one, while the simple tunnel response is a smooth function for all the excitation frequencies considered, the double-deck tunnel response presents some significant peaks at different wavenumber values. Looking at the results presented in Fig. 9 is easy to see that the peaks in the soil response are obtained at the same values where the peaks of the coupling forces where found. The only difference found now is that their relative amplitude has been modulated by the PiP receptances. The second difference is that, for high excitation frequencies, the range of wavenumber values where the soil response amplitude is significant is clearly smaller for a double-deck tunnel than for a simple tunnel. The interior floor of the tunnel prevents the propagation of waves with a short wavelength. This result is of great help for defining a wavenumber sampling that allows to compute properly the numerical inverse Fourier transform performed to obtain the response in the space domain. For example, while for high excitation frequencies an upper wavenumber value of 2 $\mathrm{rad}\cdot\mathrm{m}^{-1}$ is clearly insufficient for obtaining the response of the simple tunnel, it is clearly enough for the double-deck one.

Fig. 11 presents a comparison of the maximum displacement magnitude of both tunnels in the space domain. The results are obtained applying Eq. (3) to the previous wavenumber results and considering three different cross-sections: $x_m = 0$, 10 and 25 m. The main difference between the response of both models is that, for the case of the double-deck tunnel, significant peaks of amplitude occur for certain values of the excitation frequency. The response of the double-deck tunnel at these excitation frequencies becomes about 25 dB higher than the one of the simple tunnel. The clear differences between the response of both tunnels show that the use of the PiP model for the prediction of the response of a double-deck tunnel may give very inaccurate results. The model presented in this work allows to extend the prediction of train-induced vibrations to the case of double-deck tunnels without losing the great computational efficiency obtained using a complete analytical formulation of the problem.

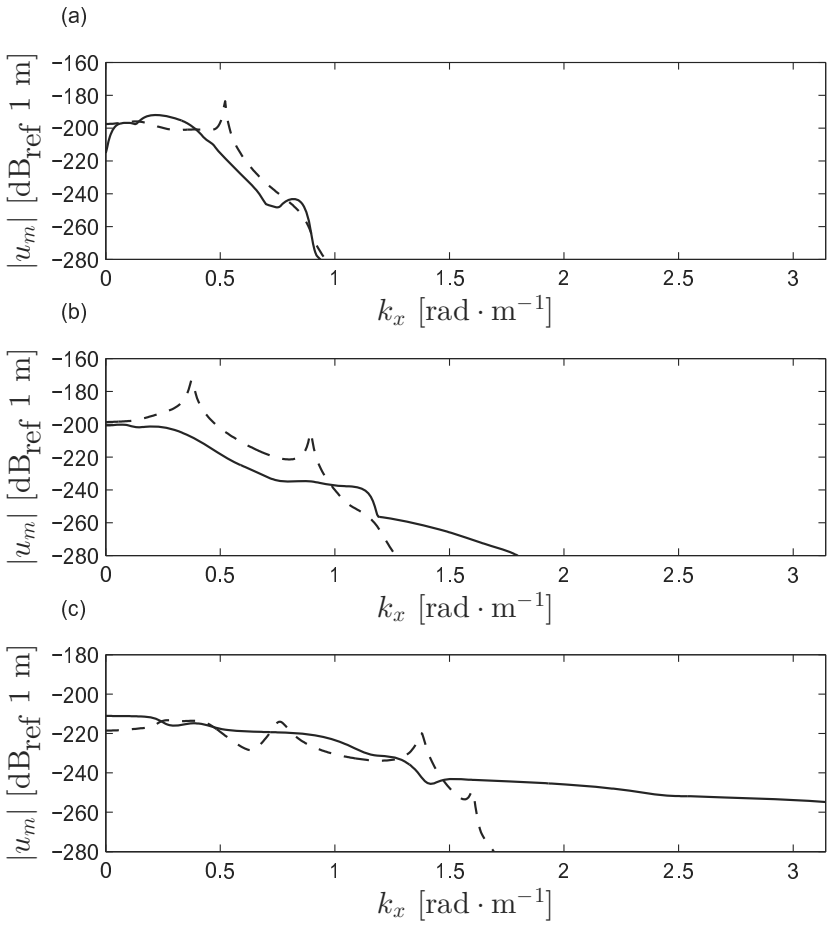

Fig. 10: Maximum displacement magnitude of a double-deck (dashed) and of a single (continuous) tunnel in the wavenumber domain. Results are presented for different exciting frequencies: (a) 20 Hz, (b) 50 Hz and (c) 150 Hz.

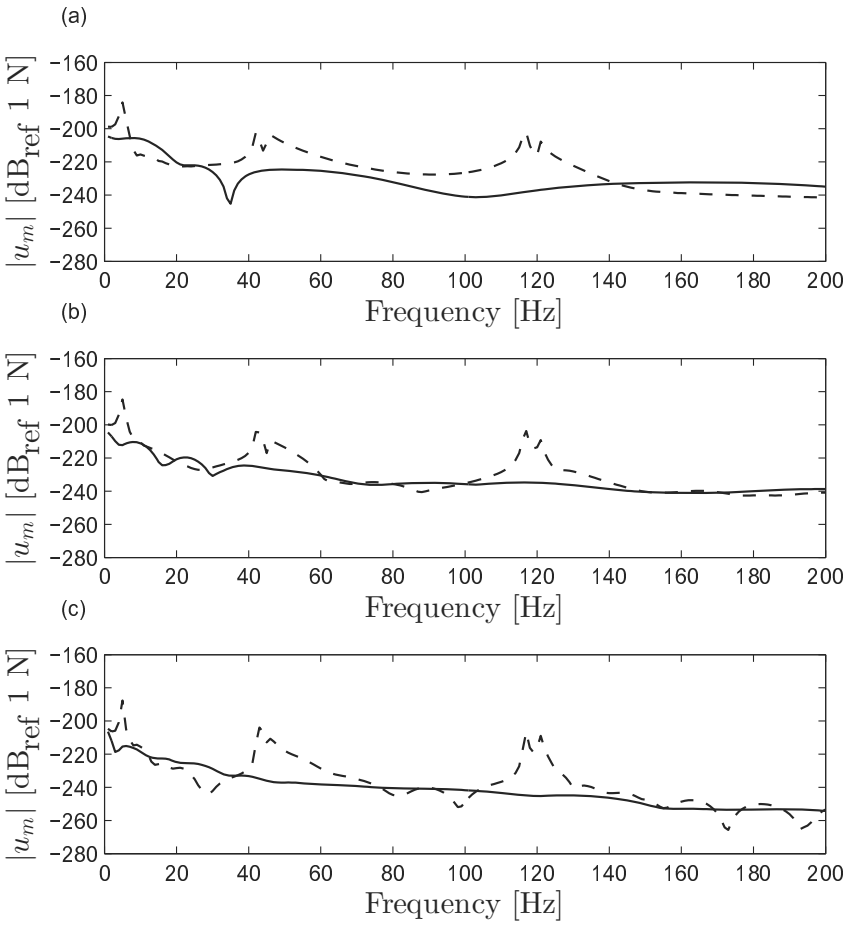

Fig. 11: Maximum displacement magnitude of a double-deck (dashed) and of a single (continuous) tunnel in the space domain. Results are presented for different cross-sections: (a) $x_m = 0$ m, (b) $x_m = 10$ m and (c) $x_m = 25$ m.

5. Conclusions

This work develops a 2.5D dynamic model of a double-deck tunnel embedded in a full-space for the prediction of underground train-induced vibrations. The response of the tunnel is obtained coupling the interior floor and the tunnel-soil subsystems in the wavenumber-frequency domain. The interior floor is represented as a thin strip plate and the tunnel-soil system is modelled using the well-known PiP model. For the case of the strip plate, the analytic results are compared to those obtained using a 2.5D FEM model, finding very good agreement between both. Alternative well-behaved expressions of the strip plate eigenfunctions are proposed in order to avoid numerical instabilities. Convergence tests have been also carried out to ensure that the parameters chosen to perform the numerical computation of the model are adequate.

The results obtained with the presented model show significant differences between the response of a simple tunnel and the one of a double-deck tunnel. These differences are shown to be caused by the effect that the strip plate dynamic behavior has on the amplitude of the coupling loads. The differences between both tunnel structures point out the need of a new model for the prediction of the ground-borne vibrations caused by trains circulating in a double-deck tunnel structure. The combined use of an analytical formulation of a strip plate and of the PiP model ensures that the presented model is computationally efficient, making the model suitable for performing predictive studies in the design stage of a new double-deck tunnel construction.

Appendix A: Antisymmetric PiP matrices

This appendix presents the PiP matrices for the antisymmetric loading formulation. The coefficient are the ones presented in Forrest and Hunt (2006b) and they are only repeated here for completeness. The matrix elements numeration used here is slightly different than the one used in their work.

The matrix $\mathbf{A_E}$, related to the thin shell, can be written as

$$\mathbf{A_E} = \frac{E_t h_t}{-r_t(1-\nu_t^2)} \begin{pmatrix} a_{11} & -a_{12} & a_{13} \\ -a_{21} & a_{22} & -a_{23} \\ a_{31} & -a_{32} & a_{33} \end{pmatrix},$$

where

$$\begin{aligned}
a_{11} &= \frac{\rho_t r_t(1-\nu_t^2)\omega^2}{E_t} - r_t k_x^2 - \frac{(1-\nu_t)n^2}{2r_t}\left(1+\frac{h_t^2}{12r_t^2}\right), \\
a_{12} &= \frac{(1+\nu_t)\mathrm{i}k_x n}{2}, \\
a_{13} &= -\nu_t \mathrm{i}k_x - \frac{h_t^2 \mathrm{i}k_x^3}{12} + \frac{h^2(1-\nu_t)\mathrm{i}k_x n^2}{24r_t^2}, \\
a_{21} &= \frac{-(1+\nu_t)\mathrm{i}k_x n}{2} = -a_{12}, \\
a_{22} &= \frac{\rho_t r_t(1-\nu_t^2)\omega^2}{E_t} - \frac{r_t(1-\nu_t)k_x^2}{2}\left(1+\frac{h_t^2}{4r_t^2}\right) - \frac{n^2}{r_t}, \\
a_{23} &= \frac{n}{r_t} + \frac{h_t^2(3-\nu_t)k_x^2 n}{24r_t}, \\
a_{31} &= \nu_t \mathrm{i}k_x + \frac{h_t^2 \mathrm{i}k_x^3}{12} - \frac{h_t^2(1-\nu_t)\mathrm{i}k_x n^2}{24r_t^2} = -a_{13}, \\
a_{32} &= \frac{n}{r_t} + \frac{h_t^2(3-\nu_t)k_x^2 n}{24r_t} = a_{23}, \\
a_{33} &= \frac{\rho_t r_t(1-\nu_t^2)\omega^2}{E_t} - \frac{h_t^2}{12}\left(r_t k_x^4 + \frac{2k_x^2 n^2}{r_t} + \frac{n^4}{r_t^3}\right) - \frac{1}{r_t} + \frac{h_t^2}{12r_t^3}(2n^2-1).
\end{aligned}$$

where E_t is the tunnel's Young modulus, ν_t is its Poissons ratio and ρ_t is the concrete density.

The matrices $\mathbf{U}$ and $\mathbf{T}$, related to the elastic continuum, take the form

$$\mathbf{U} = \begin{pmatrix} u_{31} & -u_{32} & -u_{33} \\ -u_{21} & u_{22} & u_{23} \\ -u_{11} & u_{12} & u_{13} \end{pmatrix}, \qquad \mathbf{T} = \begin{pmatrix} -t_{31} & t_{32} & t_{33} \\ t_{21} & -t_{22} & -t_{23} \\ t_{11} & -t_{12} & -t_{13} \end{pmatrix},$$

where

$$\begin{aligned}
u_{11} &= \frac{n}{r}K_n(\nu_P r) - \nu_P K_{n+1}(\nu_P r),\\
u_{12} &= \mathrm{i}k_x K_{n+1}(\nu_S r),\\
u_{13} &= \frac{n}{r}K_n(\nu_S r),\\
u_{21} &= \frac{-n}{r}K_n(\nu_P r),\\
u_{22} &= \mathrm{i}k_x K_{n+1}(\nu_S r),\\
u_{23} &= -\frac{n}{r}K_n(\nu_S r) + \nu_S K_{n+1}(\nu_S r),\\
u_{31} &= \mathrm{i}k_x K_n(\nu_P r),\\
u_{32} &= \nu_S K_n(\nu_S r),\\
u_{33} &= 0.
\end{aligned}$$

$$\begin{aligned}
t_{11} &= \left(2\mu_s\frac{n^2-n}{r^2} - \lambda_s k_x^2 + (\lambda_s+2\mu_s)\nu_P^2\right)K_n(\nu_P r) + 2\mu_s\frac{\nu_P}{r}K_{n+1}(\nu_P r),\\
t_{12} &= -2\mu_s\mathrm{i}k_x\nu_S K_n(\nu_S r) - 2\mu_s\mathrm{i}k_x\frac{n+1}{r}K_{n+1}(\nu_S r),\\
t_{13} &= 2\mu_s\frac{n^2-n}{r^2}K_n(\nu_S r) - 2\mu_s\frac{n}{r}\nu_S K_{n+1}(\nu_S r),\\
t_{21} &= -2\mu_s\frac{n^2-n}{r^2}K_n(\nu_P r) + 2\mu_s\frac{n}{r}\nu_P K_{n+1}(\nu_P r),\\
t_{22} &= -\mu_s\mathrm{i}k_x\nu_S K_n(\nu_S r) - 2\mu_s\mathrm{i}k_x\frac{n+1}{r}K_{n+1}(\nu_S r),\\
t_{23} &= \left(-2\mu_s\frac{n^2-n}{r^2} - \mu_s\nu_S^2\right)K_n(\nu_S r) - 2\mu_s\frac{\nu_S}{r}K_{n+1}(\nu_S r),\\
t_{31} &= 2\mu_s\mathrm{i}k_x\frac{n}{r}K_n(\nu_P r) - 2\mu_s\mathrm{i}k_x\nu_P K_{n+1}(\nu_P r),\\
t_{32} &= \mu_s\frac{n}{r}\nu_S K_n(\nu_S r) - \mu_s(k_x^2+\nu_S^2)K_{n+1}(\nu_S r),\\
t_{33} &= \mu_s\mathrm{i}k_x\frac{n}{r}K_n(\nu_S r).
\end{aligned}$$

where K_n is the modified Bessel function of the second kind and order n, λ_s and μ_s are the first and second Lamé coefficients and where

$$\nu_P = \sqrt{k_x^2 - \frac{\omega^2}{c_P^2}}, \quad \nu_S = \sqrt{k_x^2 - \frac{\omega^2}{c_S^2}}.$$

The values of c_P and c_S, which are the P-wave and S-wave velocities respectively, are given by

$$c_P = \sqrt{\frac{(\lambda_s + 2\mu_s)(1 + 2\mathrm{i}D_P)}{\rho_s}}, \quad c_S = \sqrt{\frac{\mu_s(1 + 2\mathrm{i}D_S)}{\rho_s}},$$

where ρ_s is the soil density and D_P and D_S are the hysteretic damping ratios of both types of waves.

Acknowledgements

Part of the presented research has been carried out while the first author was holding a FPU-UPC doctoral student grant. The author wants to express his gratitude to the Universitat Politècnica de Catalunya (UPC) for this financial support.

References

References

Andersen, L. and Jones, C.J.C., 2006. Coupled boundary and finite element analysis of vibration from railway tunnels–a comparison of two- and three-dimensional models. J. Sound. Vib. 293, 611 – 625.

Aubry, D., Clouteau, D., Bonnet, G., 1994. Modelling of wave propagation due to fixed or mobile dynamic sources, in: Workshop Wave '94, Wave propagation and Reduction of Vibrations.

Broere, W., 2016. Urban underground space : Solving the problems of today's cities. Tunn. Undergr. Sp. Tech. 55, 245–248.

Chua, K.H., Balendra, T., Lo, K.W., 1992. Groundborne vibrations due to trains in tunnels. Earthq. Eng. Struct. D. 21, 445–460.

Clot, A., 2014. A dynamical model of a double-deck circular tunnel embedded in a full-space. Ph.D. thesis.

Clot, A., Romeu, J., Arcos, R., Martín, S.R., 2014. A power flow analysis of a double-deck circular tunnel embedded in a full-space. Soil Dyn. Earthq. Eng. 57, 1–9.

Clouteau, D. and Arnst, M. and Al-Hussaini, T. M. and Degrande, G., 2005. Freefield vibrations due to dynamic loading on a tunnel embedded in a stratified medium. J. Sound. Vib. 283, 173 – 199.

Degrande, G., Clouteau, D., Othman, R., Arnst, M., Chebli, H., Klein, R., Chatterjee, P., Janssens, B., 2006. A numerical model for ground-borne vibrations from underground railway traffic based on a periodic finite element-boundary element formulation. J. Sound. Vib. 293, 645–666.

Forrest, J., Hunt, H., 2006a. Ground vibration generated by trains in underground tunnels. J. Sound. Vib. 294, 706–736.

Forrest, J., Hunt, H., 2006b. A three-dimensional tunnel model for calculation of train-induced ground vibration. J. Sound. Vib. 294, 678–705.

François, S., Schevenels, M., Galvín, P., Lombaert, G., Degrande, G., 2010. A 2.5D coupled FE-BE methodology for the dynamic interaction between longitudinally invariant structures and a layered halfspace. Comput. Method. Appl. M. 199, 1536–1548.

Gonçalves, P., Brennan, M., Elliott, S., 2007. Numerical evaluation of high-order modes of vibration in uniform Euler-Bernoulli beams. J. Sound. Vib. 301, 1035–1039.

Graff, K., 1975. Wave Motion in Elastic Solids. Oxford University Press.

Gupta, S., Hussein, M., Degrande, G., Hunt, H., Clouteau, D., 2007. A comparison of two numerical models for the prediction of vibrations from underground railway traffic. Soil Dyn. Earthq. Eng. 27, 608–624.

Hussein, M., François, S., Schevenels, M., Hunt, H., Talbot, J., Degrande, G., 2014. The fictitious force method for efficient calculation of vibration from a tunnel embedded in a multi-layered half-space. J. Sound. Vib. 333, 6996–7018.

Hussein, M., Gupta, S., Hunt, H., Degrande, G., Talbot, J., 2006. An efficient model for calculating vibration from a railway tunnel buried in a half-space, in: Proceedings of the Thriteenth International Congress on Sound and Vibration, Vienna.

Hussein, M., Hunt, H., 2007. A numerical model for calculating vibration from a railway embedded in a full-space. J. Sound. Vib. 305, 401–431.

ISO 14837-1:2005, . Mechanical vibration. Ground-borne noise and vibration arising from rail systems. Part 1: General Guidance.

Lee, Y., Choi, M., 2001. Free vibrations of circular cylindrical shells with an interior plate using the receptance method. J. Sound. Vib. 248, 477–497.

Lee, Y., Choi, M., Kim, J., 2003. Free vibrations of laminated composite cylindrical shells with an interior rectangular plate. J. Sound. Vib. 265, 795–817.

Leissa, A., 1993. Vibration of plates. Acoustical Society of America.

Li, X.G., Yuan, D.J., 2012. Response of a double-decked metro tunnel to shield driving of twin closely under-crossing tunnels. Tunn. Undergr. Sp. Tech. 28, 18–30.

Müller, K., Grundmann, H., Lenz, S., 2008. Nonlinear interaction between a moving vehicle and a plate elastically mounted on a tunnel. J. Sound. Vib. 310, 558–586.

Nejati, H.R. and Ahmadi, M. and Hashemolhosseini, H., 2012. Numerical analysis of ground surface vibration induced by underground train movement. Tunn. Undergr. Sp. Tech. 29, 1 – 9.

Peterson, M., Boyd, D., 1978. Free vibrations of circular-cylinders with longitudinal, interior partitions. J. Sound. Vib. 60, 45–62.

Real, T., Zamorano, C., Ribes, F., Real, J.I., 2015. Train-induced vibration prediction in tunnels using 2D and 3D FEM models in time domain. Tunn. Undergr. Sp. Tech. 49, 376–383.

Shampine, L.F., 2008. Vectorized adaptive quadrature in MATLAB. J. Comput. Appl. Math. 211, 131–140.

Sheng, X., Jones, C., Thompson, D., 2005. Modelling ground vibration from railways using wavenumber finite- and boundary-element methods. Proc. R. Soc. A 461, 2043–2070.

Söedel, W., 1993. Vibration of Shells and Plates. volume 86 of *Mechanical Engineering*. Marcel Dekker.

Tadeu, A., António, J., Godinho, L., 2001. Green's function for two-and-a-half dimensional elastodynamic problems in a half-space. Comput. Mech. 27, 484–491.

Tadeu, A., Kausel, E., 2000. Green's functions for two-and-a-half-dimensional elastodynamic problems. J. Eng. Mech. ASCE 126, 1093–1097.

Wang, Z., Xing, J., Price, W., 2004. A study of power flow in a coupled plate-cylindrical shell system. J. Sound. Vib. 271, 863–882.

Zhao, Z., Sheng, M., Yang, Y., 2012. Vibration Transmission of a Cylindrical Shell with an Interior Rectangular Plate with the Receptance Method. Adv. Acoust. Vib. 2012, 1–9.

List of Figures

List of Tables